

RESEARCH ARTICLE

Open Access



# LBSizeClev: improved support vector machine (SVM)-based prediction of Dicer cleavage sites using loop/bulge length

Yu Bao<sup>\*</sup>, Morihito Hayashida and Tatsuya Akutsu

## Abstract

**Background:** Dicer is necessary for the process of mature microRNA (miRNA) formation because the Dicer enzyme cleaves pre-miRNA correctly to generate miRNA with correct seed regions. Nonetheless, the mechanism underlying the selection of a Dicer cleavage site is still not fully understood. To date, several studies have been conducted to solve this problem, for example, a recent discovery indicates that the loop/bulge structure plays a central role in the selection of Dicer cleavage sites. In accordance with this breakthrough, a support vector machine (SVM)-based method called PHDClev was developed to predict Dicer cleavage sites which outperforms other methods based on random forest and naive Bayes. PHDClev, however, tests only whether a position in the shift window belongs to a loop/bulge structure.

**Result:** In this paper, we used the length of loop/bulge structures (in addition to their presence or absence) to develop an improved method, LBSizeClev, for predicting Dicer cleavage sites. To evaluate our method, we used 810 empirically validated sequences of human pre-miRNAs and performed fivefold cross-validation. In both 5p and 3p arms of pre-miRNAs, LBSizeClev showed greater prediction accuracy than PHDClev did. This result suggests that the length of loop/bulge structures is useful for prediction of Dicer cleavage sites.

**Conclusion:** We developed a novel algorithm for feature space mapping based on the length of a loop/bulge for predicting Dicer cleavage sites. The better performance of our method indicates the usefulness of the length of loop/bulge structures for such predictions.

**Keywords:** Dicer cleavage site, Support vector machine, Loop/bulge length

## Background

MicroRNAs (miRNAs) are a type of small RNAs with the length ~22 nt, which perform the function of suppressing gene expression at the post-transcriptional level [1, 2]. Usually in vivo, a gene of a miRNA is transcribed to produce a long, primary miRNA (pri-miRNA) transcript, which is then processed into a ~65-nt-long hairpin structure via cleavage by the Drosha (DGCR8) enzyme. Then, the resulting pre-miRNA is cleaved by another enzyme (termed Dicer) to generate a mature miRNA, which is ~22 nt long [3]. Finally, the generated miRNA can be combined with an Argonaute protein to form the protein-miRNA

complex, which can control various cellular progresses including development, cell death, and metabolism [4–6].

Dicer is a 1922-amino acid multidomain protein that belongs to the RNase III family. Dicer generally contains several domains including ATPase-helicase, DUF283 (a double-stranded-RNA-binding domain), PAZ (Piwi-Argonaute-Zwille) domain, two RNase III domains, and a dsRBD [7]. Dicer in various species may contain a different combination of these domains. Among these domains, the PAZ domain, RNase III domain, and dsRND are responsible for the function of substrate cleavage [8]. The cleavage occurs near the end of the terminal loop of pre-miRNA, introducing a cut into the hairpin.

Structural analysis of human Dicer revealed that the PAZ domain contains a 5p phosphate-binding pocket, which may be necessary for selection of a Dicer cleavage

<sup>\*</sup>Correspondence: houu@kuicr.kyoto-u.ac.jp  
Laboratory of Mathematical Bioinformatics, Bioinformatics Center, Institute for Chemical Research, Kyoto University, Gokasho, Uji, 611-0011 Kyoto, Japan

site [9]. There are also studies showing that the loop/bulge structure also determines the accuracy of cleavage activity [10, 11]. MacRae et al. reported that the 3p-terminal nucleotide of single-stranded RNA can affect Dicer binding [12]. In addition, Jin and Lee found that a single nucleotide polymorphism may be associated with miRNA regulation [13]. All these studies revealed that secondary structures of both the Dicer enzyme and cleavage substrates are essential for cleavage site determination.

With a better understanding of the features of selection of a Dicer cleavage site, researchers may be able to elucidate the mechanism of action of enzymes in the RNA III family as well as the processes of RNA inference. Thus, it is imperative to explore the factors affecting the accuracy of Dicer cleavage to gain better insights into the mechanism of Dicer cleavage. Recently, a support vector machine (SVM)-based method (PHDCleav) was developed to predict selection of Dicer cleavage sites [14]. They proposed feature space mappings from pre-miRNA nucleotide sequences on the basis of existence of a predicted loop/bulge structure. SVM is a state-of-the-art machine learning technology [15] that has been applied to various areas of pattern recognition in many biological fields such as protein classification [16–18], prediction of RNA secondary structure [19, 20], and drug–nondrug classification [21, 22].

In this paper, we made use of the length of loop/bulge structures and proposed a novel algorithm of feature space mapping called *LBSizeCleav*. To evaluate our method, we used 810 empirically valid sequences of pre-miRNAs from miRBase and performed fivefold cross-validation. In the 5p arm of pre-miRNAs, the proposed method attained higher accuracy (87.4%), whereas the best prediction result of PHDCleav corresponded to the accuracy of 84.0% (an extended binary pattern, a window of 14-nt size). In addition, in the 3p arm, the average prediction accuracy of our method reached 83.0%, whereas PHDCleav achieved up to 79.1% prediction accuracy. These results suggest that our method *LBSizeCleav* outperforms binary patterns of PHDCleav in predicting the position of Dicer cleavage sites. The better performance may in turn serve as the evidence that the features utilized by these two methods are necessary for Dicer cleavage selection.

### Methods

In this section, we provide a brief description of feature space mapping algorithms of PHDCleav using sequences and secondary structures and propose a novel algorithm for feature space mapping, *LBSizeCleav*, based on the length of a loop/bulge structure.

#### Feature space mapping procedures of PHDCleav

Given a pre-miRNA sequence, a site between two successive nucleotides is mapped to a binary vector. In

PHDCleav, a window is generated for each input sequence where for the positive pattern the center of the window is exactly located at the cleavage site of 5p (3p) arm and for the negative pattern the center of the window is located 6 nt away from the cleavage site of 5p(3p) arm. Since this is based on the assumption that a cleavage site can shift slightly (1-2 nt in biological experiments) but the chance is rare that Dicer cuts in the middle of mature miRNA, 6 nt could be changed under the principle that the center of the negative pattern is far enough from the real cleavage site. PHDCleav has shown that there is little affect to the accuracy of prediction even with the shifting of negative windows among the whole sequence of pre-miRNA.

A nucleotide in a window having the site at the center is converted to a four-dimensional vector as [1, 0, 0, 0], [0, 1, 0, 0], [0, 0, 1, 0], and [0, 0, 0, 1], for A, U, C, and G, respectively (see Table 1). Let  $w$  denote the size of the window, where  $w$  is a positive even number. Then, a  $4w$ -dimensional vector is generated for the site.

There are many loops/bulges in the secondary structure of pre-miRNA where one arm contains extra nucleotides without counterparts in the other arm [23]. A recent study indicated that these loops/bulges play an important role in the selection of a Dicer cleavage site [10]. This observation

**Table 1** Binary patterns for nucleotides, A, U, C, G, and a loop/bulge structure, denoted by L, in PHDCleav [14] and *LBSizeCleav* with  $k$  ones based on sequences and predicted secondary structures

Mapping	Sequence	Structure
PHDCleav	A	[1, 0, 0, 0]
	U	[0, 1, 0, 0]
	C	[0, 0, 1, 0]
	G	[0, 0, 0, 1]
	L	—
Extended PHDCleav	A	[1, 0, 0, 0, 0]
	U	[0, 1, 0, 0, 0]
	C	—
	G	[0, 0, 0, 1, 0]
	L	[0, 0, 0, 0, 1]
<i>LBSizeCleav</i>	A	[1, 0, 0, 0, 0, ..., 0]
	U	[0, 1, 0, 0, 0, ..., 0]
	C	—
	G	[0, 0, 0, 1, 0, ..., 0]
	L	[0, 0, 0, 0, 0, ..., 0, $\overbrace{1, \dots, 1}^k$ , 0, ...]

In PHDCleav binary patterns each nucleotide is represented by a 4-dimensional vector, and in PHDCleav Extended patterns each nucleotide is represented by a 5-dimensional vector, while in *LBSizeCleav* the dimension of the vector is  $3 + k + N$ , in which  $N$  denotes the maximum number of length of loop/bulges among all the pre-miRNAs in the training dataset

suggests that the loop/bulge structure may be a feature that is useful for prediction of a Dicer cleavage site. The extended binary pattern of PHDCleav was developed on the basis of this assumption.

After obtaining the secondary structure from a given sequence by some prediction methods, in the extended binary pattern of PHDCleav, a nucleotide is converted to a five-dimensional vector as [1, 0, 0, 0, 0], [0, 1, 0, 0, 0], [0, 0, 1, 0, 0], [0, 0, 0, 1, 0], and [0, 0, 0, 0, 1], for A, U, C, G, and L, respectively, where L indicates that the corresponding nucleotide is predicted to be in a loop/bulge structure. Just as the nucleotides in the window, its complementary nucleotides are also converted to a feature vector. After that, the dimensionality of the vector is 10w.

**Feature space mapping of LBSizeCleav**

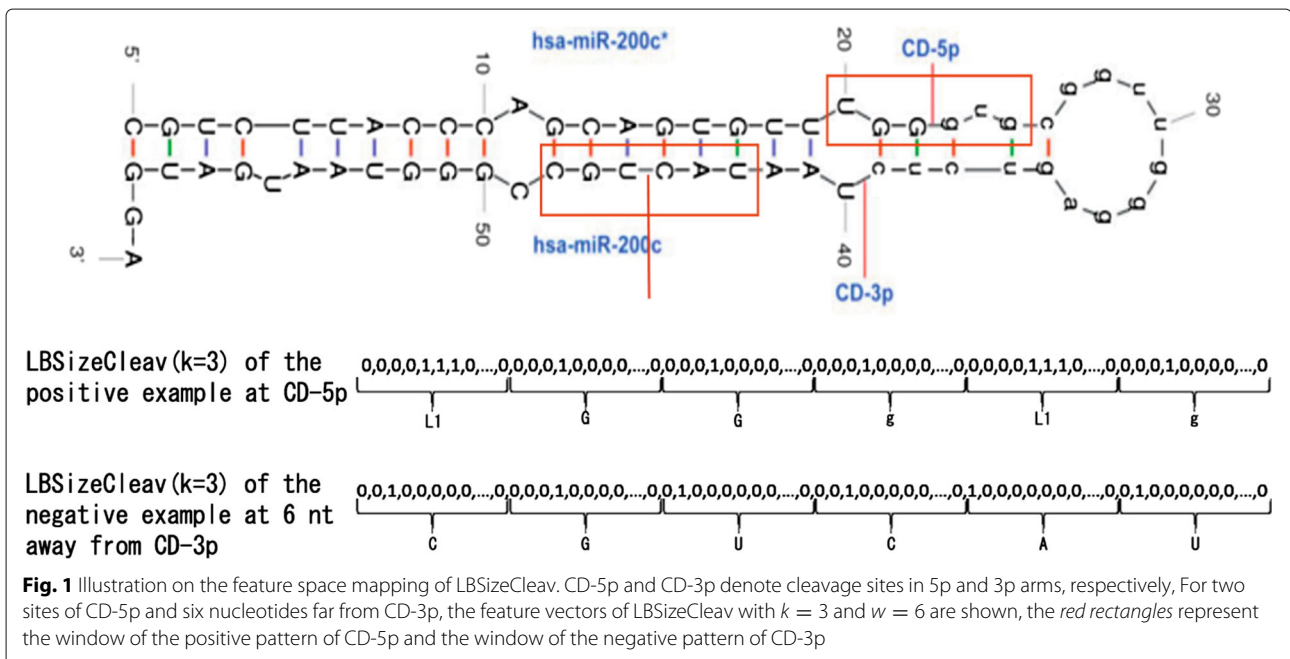
It is reasonable to consider not only the position but also the length of loop/bulge structures. Therefore, we propose novel feature space mapping (LBSizeCleav) by introducing the length of a loop/bulge structure into the algorithm.

The binary pattern of LBSizeCleav is an extension of that of PHDCleav. Let  $M$  be the maximal length of loops and bulges of all the pre-miRNAs in a dataset, and suppose  $L_l$  indicates that the corresponding nucleotide is in a loop/bulge structure of length  $l$ . Here we introduce a new parameter named  $k$  into LBSizeCleav, which is a positive integer representing the effect of length of loops and bulges to the kernel computation. Then, we designate a nucleotide without any loop/bulge structure for  $k$  as a  $(M + k + 3)$ -dimensional vector, namely, [1, 0, 0, 0, ..., 0], [0, 1, 0, 0, ..., 0], [0, 0, 1, 0, 0, ..., 0], [0, 0, 0, 1, 0, ..., 0] for A, U, C, and G, respectively (see Table 1). A nucleotide

in a loop/bulge structure of length  $l$  is represented as [0, ..., 0, 1, ..., 1, 0, ...], where  $k$  ones appear from the  $(4 + l)$ -th element to the  $(k + 3 + l)$ -th element. Thus, for window size  $w$ , a  $2w(M + k + 3)$ -dimensional vector is generated.

Let  $x_1$  and  $x_2$  be binary patterns of  $L_{l_1}$  and  $L_{l_2}$ , respectively. If we use the inner product for kernel computation, then the inner product between the binary patterns is  $x_1 \cdot x_2 = \max\{k - |l_1 - l_2|, 0\}$ . If we use the radial basis function (RBF) kernel,  $\exp\{-\gamma \|x_1 - x_2\|^2\} = \exp\{-4\gamma \min\{(l_1 - l_2)^2, k^2\}\}$ , where  $\gamma > 0$ . These values assume the maximum when  $l_1 = l_2$  and decrease according to the difference  $|l_1 - l_2|$  and  $k$ , while  $k$  gets larger, the value changes of kernel function is more sensitive to the size of  $|l_1 - l_2|$ , in this way by controlling the value  $k$  we could control the sensitivity of our method to length of loops and bulges. Since PHDCleav used radial basis function (RBF), we also selected RBF as our kernel function.

Figure 1 illustrates the feature space mapping of LBSizeCleav for the pre-miRNA of the miRBase ID hsa-miR-200c with a predicted secondary structure, where nucleotides in the region removed by Dicer are shown as lowercase letters. CD-5p and CD-3p denote cleavage sites in 5p and 3p arms, respectively. Sequences in the red rectangles denote sequences used to generate feature vectors representing 5p and 3p arms, which are selected by the principle that the cleavage site is located at the center of the sequence. Here, we generate the feature vector of LBSizeCleav at  $k = 3$  and  $w = 6$  for the site CD-5p and for the site 6 nt away from CD-5p. The nucleotides in the window in the 5p arm are UGGgug, and loop/bulge structures are detected at two positions. As a result,  $L_1GGgL_1g$  is converted to



the  $6(M+6)$ -dimensional binary vector, where loop/bulge structures  $L_l$  are inserted. For the 3p arm, CGUCAU is converted in accordance with Table 1.

### Results

We retrieved 810 empirically validated sequences of pre-miRNAs from miRBase (version 21) [24], where cleavage

sites CD-5p and CD-3p are both defined for each pre-miRNA. The pre-miRNAs were selected under the principle that both the cleavage sites of CD-5p and CD-3p are experimentally validated. (i.e. only precursors with cleavage sites at both CD-5p and CD-3p are selected, we made this choice to let our dataset be generated the in same way as dataset of PHDCleav)

**Table 2** Results on average specificity, sensitivity, accuracy, and MCC for both 5p and 3p arms by five-fold cross-validation using PHDCleav and LBSIZEcleav ( $k = 1, \dots, 5$ ) with window sizes 8, 10, 12, 14 based on sequences and secondary structures predicted by quikfold server

Method	Window size	5p arm				3p arm			
		Sn	Sp	Ac	MCC	Sn	Sp	Ac	MCC
PHDCleav (sequence)	8	0.602	0.503	0.552	0.105	0.662	0.625	0.644	0.287
	10	0.541	0.573	0.557	0.115	0.661	0.642	0.652	0.303
	12	0.560	0.555	0.557	0.115	0.660	0.656	0.658	0.316
	14	0.539	0.572	0.555	0.111	0.654	0.702	0.678	0.356
PHDCleav (structure)	8	0.753	0.814	0.784	0.568	0.670	0.661	0.665	0.330
	10	0.784	0.827	0.806	0.612	0.702	0.719	0.710	0.421
	12	0.790	0.842	0.816	0.633	0.739	0.764	0.752	0.503
	14	0.799	0.857	0.828	0.657	0.779	0.783	0.781	0.562
Extended PHDCleav	8	0.750	0.798	0.774	0.548	0.652	0.716	0.684	0.369
	10	0.779	0.827	0.803	0.607	0.674	0.783	0.729	0.460
	12	0.809	0.845	0.827	0.654	0.714	0.790	0.752	0.506
	14	0.813	0.868	0.840	0.682	<b>0.781</b>	0.801	0.791	0.582
LBSIZEcleav ( $k = 1$ )	8	0.668	0.924	0.796	0.612	0.630	0.684	0.657	0.315
	10	0.709	0.947	0.828	0.675	0.651	0.776	0.713	0.430
	12	0.774	0.945	0.859	0.730	0.686	0.847	0.766	0.540
	14	0.808	0.933	0.871	0.747	0.758	0.874	0.816	0.637
LBSIZEcleav ( $k = 2$ )	8	0.662	<b>0.954</b>	0.808	0.645	0.626	0.723	0.674	0.351
	10	0.725	0.946	0.835	0.688	0.642	0.806	0.724	0.455
	12	0.784	0.938	0.861	0.731	0.665	0.882	0.773	0.560
	14	0.820	0.925	0.872	<b>0.749</b>	0.734	0.916	0.825	0.661
LBSIZEcleav ( $k = 3$ )	8	0.692	0.949	0.821	0.664	0.619	0.735	0.677	0.356
	10	0.752	0.941	0.846	0.706	0.618	0.822	0.720	0.450
	12	0.803	0.932	0.867	0.741	0.635	0.914	0.774	0.571
	14	0.825	0.912	0.869	0.740	0.719	<b>0.942</b>	<b>0.830</b>	<b>0.678</b>
LBSIZEcleav ( $k = 4$ )	8	0.695	0.949	0.822	0.667	0.614	0.736	0.675	0.353
	10	0.767	0.938	0.853	0.716	0.621	0.835	0.728	0.467
	12	0.815	0.927	0.871	0.747	0.639	0.912	0.776	0.573
	14	0.835	0.909	0.872	0.746	0.723	0.924	0.823	0.660
LBSIZEcleav ( $k = 5$ )	8	0.700	0.947	0.824	0.668	0.594	0.771	0.682	0.371
	10	0.772	0.936	0.854	0.717	0.578	0.862	0.720	0.459
	12	0.821	0.924	0.872	<b>0.749</b>	0.634	0.921	0.777	0.579
	14	<b>0.838</b>	0.909	<b>0.874</b>	<b>0.749</b>	0.724	0.932	0.828	0.671

Sn, Sp, Ac, and MCC denote sensitivity, specificity, accuracy, and Matthews correlation coefficient, respectively

All the pre-miRNAs are selected from human pre-miRNAs.

We used these cleavage sites as positive examples using windows of size 8,10,12,14 nt, where each window was selected so that a cleavage site is located at the center of the window, and we generated negative examples on the same sequence so that both centers of the positive and negative examples were 6 nt away from each other, as in the previous study [14]. This approach is based on the assumption that for most pre-miRNAs, the Dicer cleavage site is seldom selected at the center of the hairpin structure. In PHDCleav, two secondary structure predictors, quikfold [25] and RNAFold from ViennaRNA [26] were used, hence, we used both the RNAFold from ViennaRNA and the quikfold server (version 3.0, <http://mfold.rna.albany.edu/?q=DINAMelt/Quickfold>) for prediction of RNA secondary structures. The results were given in Tables 2 and 3. Because in PHDCleav, the accuracy of

prediction by nucleotide composition was worse than that by binary patterns, we compared our method with the binary patterns of PHDCleav. We used the libSVM 3.18 package [27] with the RBF kernel to utilize SVM because the RBF kernel was used in PHDCleav.

The performance of prediction methods was assessed by means of sensitivity, specificity, accuracy, and the Matthews correlation coefficient (MCC), defined as follows:

$$sensitivity = \frac{TP}{TP + FN}, \tag{1}$$

$$specificity = \frac{TN}{TN + FP}, \tag{2}$$

$$accuracy = \frac{TP + TN}{TP + FP + TN + FN}, \tag{3}$$

$$MCC = \frac{TP \cdot TN - FP \cdot FN}{\sqrt{(TP+FP)(TP+FN)(TN+FP)(TN+FN)}}, \tag{4}$$

**Table 3** Results on average specificity, sensitivity, accuracy, and MCC for both 5p and 3p arms by five-fold cross-validation using PHDCleav and LBSIZEcleav ( $k = 1, \dots, 5$ ) with window sizes 8, 10, 12, 14 based on secondary structures predicted by RNAFold

Method	Window size	5p arm				3p arm			
		Sn	Sp	Ac	MCC	Sn	Sp	Ac	MCC
Extended PHDCleav	8	0.746	0.744	0.745	0.490	0.772	0.750	0.761	0.522
	10	0.792	0.783	0.787	0.575	0.779	0.800	0.790	0.580
	12	0.798	0.799	0.798	0.597	0.785	0.830	0.808	0.616
	14	0.778	0.813	0.795	0.591	0.805	<b>0.853</b>	0.829	0.659
LBSIZEcleav ( $k = 1$ )	8	0.739	0.805	0.772	0.545	0.785	0.790	0.788	0.576
	10	0.798	0.820	0.809	0.618	0.795	0.815	0.805	0.610
	12	0.792	0.815	0.803	0.607	0.822	0.840	0.831	0.662
	14	0.815	<b>0.822</b>	<b>0.819</b>	<b>0.638</b>	0.851	0.852	<b>0.851</b>	<b>0.703</b>
LBSIZEcleav ( $k = 2$ )	8	0.753	0.788	0.771	0.542	0.792	0.788	0.790	0.580
	10	0.816	0.795	0.806	0.612	0.811	0.794	0.803	0.606
	12	0.836	0.784	0.810	0.621	0.814	0.803	0.808	0.617
	14	0.845	0.769	0.807	0.616	0.867	0.800	0.834	0.669
LBSIZEcleav ( $k = 3$ )	8	0.751	0.794	0.773	0.546	0.784	0.797	0.790	0.581
	10	0.808	0.808	0.808	0.615	0.795	0.813	0.804	0.608
	12	0.822	0.800	0.811	0.623	0.808	0.835	0.821	0.643
	14	0.816	0.803	0.809	0.619	0.853	0.838	0.846	0.692
LBSIZEcleav ( $k = 4$ )	8	0.764	0.772	0.768	0.536	0.809	0.772	0.790	0.581
	10	0.824	0.762	0.793	0.587	0.824	0.766	0.795	0.590
	12	0.841	0.737	0.789	0.581	0.842	0.756	0.799	0.600
	14	0.871	0.678	0.774	0.559	0.898	0.697	0.797	0.607
LBSIZEcleav ( $k = 5$ )	8	0.782	0.747	0.764	0.529	0.822	0.744	0.783	0.568
	10	0.836	0.732	0.784	0.572	0.829	0.726	0.777	0.558
	12	0.867	0.699	0.783	0.574	0.864	0.682	0.773	0.556
	14	<b>0.899</b>	0.626	0.763	0.546	<b>0.917</b>	0.619	0.768	0.562

Sn, Sp, Ac, and MCC denote sensitivity, specificity, accuracy, and Matthews correlation coefficient, respectively

where  $TP, TN, FP, FN$  denote the number of true positive, true negative, false positive, and false negative results, respectively.

We performed fivefold cross-validation, and used the average sensitivity, specificity, accuracy, and MCC. We examined size  $w$  of a window from 8 to 14 and the number  $k$  of ones in LBSizeCleave from 1 to 5 for 5p and 3p

arms of pre-miRNAs. Table 2 shows the results of PHDCleave and LBSizeCleave ( $k = 1, \dots, 5$ ) based on sequences and secondary structures predicted by the quikfold server. In terms of prediction performance in the 5p arm of pre-miRNA, the best result of PHDCleave corresponded to the accuracy of 84.0%, whereas LBSizeCleave at  $k = 5$  achieved the accuracy of 87.4%. In addition, the values

**Table 4** Variances of specificity, sensitivity, accuracy, and MCC for both 5p and 3p arms by five-fold cross-validation using PHDCleave and LBSizeCleave ( $k = 1, \dots, 5$ ) with window sizes 8, 10, 12, 14 based on sequences and secondary structures predicted by quikfold server

feature extraction method	Window size	CD-5p				CD-3p			
		Sn	Sp	Ac	Mc	Sn	Sp	Ac	Mc
PHDCleave (sequence)	8	0.0137	0.0008	0.0074	0.0036	0.0072	0.0015	0.0094	0.0066
	10	0.0184	0.0004	0.0111	0.0018	0.0044	0.0005	0.0072	0.0024
	12	0.0208	0.0001	0.0223	0.0003	0.0078	0.0011	0.0031	0.0046
	14	0.0293	0.0009	0.0174	0.0037	0.0065	0.0007	0.0048	0.0029
PHDCleave (structure)	8	0.0042	0.0039	0.0067	0.0155	0.0187	0.0013	0.0091	0.0062
	10	0.0026	0.0043	0.0088	0.0177	0.0100	0.0014	0.0050	0.0059
	12	0.0042	0.0027	0.0034	0.0109	0.0051	0.0011	0.0024	0.0045
	14	0.0047	0.0031	0.0034	0.0125	0.0039	0.0012	0.0014	0.0047
Extended PHDCleave	8	0.0029	0.0032	0.0063	0.0128	0.0123	0.0025	0.0043	0.0103
	10	0.0030	0.0038	0.0061	0.0154	0.0064	0.0019	0.0016	0.0075
	12	0.0040	0.0033	0.0050	0.0136	0.0054	0.0015	0.0011	0.0059
	14	0.0059	0.0027	0.0016	0.0108	0.0032	0.0013	0.0010	0.0052
LBSizeCleave( $k = 1$ )	8	0.0030	0.0025	0.0044	0.0115	0.0100	0.0004	0.0074	0.0019
	10	0.0022	0.0015	0.0013	0.0064	0.0078	0.0011	0.0015	0.0042
	12	0.0050	0.0024	0.0010	0.0090	0.0077	0.0015	0.0002	0.0051
	14	0.0075	0.0035	0.0010	0.0132	0.0036	0.0007	0.0002	0.0026
LBSizeCleave( $k = 2$ )	8	0.0042	0.0018	0.0008	0.0066	0.0053	0.0010	0.0036	0.0041
	10	0.0038	0.0020	0.0009	0.0076	0.0034	0.0010	0.0010	0.0039
	12	0.0051	0.0029	0.0016	0.0115	0.0042	0.0017	0.0008	0.0063
	14	0.0051	0.0028	0.0012	0.0107	0.0043	0.0008	0.0002	0.0024
LBSizeCleave( $k = 3$ )	8	0.0025	0.0013	0.0008	0.0050	0.0070	0.0010	0.0021	0.0042
	10	0.0039	0.0022	0.0012	0.0086	0.0064	0.0013	0.0006	0.0048
	12	0.0063	0.0031	0.0012	0.0119	0.0039	0.0015	0.0005	0.0055
	14	0.0060	0.0033	0.0015	0.0130	0.0073	0.0016	0.0003	0.0046
LBSizeCleave( $k = 4$ )	8	0.0029	0.0016	0.0009	0.0064	0.0066	0.0020	0.0030	0.0078
	10	0.0046	0.0025	0.0011	0.0095	0.0071	0.0014	0.0006	0.0049
	12	0.0061	0.0032	0.0014	0.0124	0.0033	0.0011	0.0007	0.0041
	14	0.0051	0.0030	0.0015	0.0120	0.0088	0.0025	0.0002	0.0082
LBSizeCleave( $k = 5$ )	8	0.0029	0.0017	0.0009	0.0066	0.0062	0.0021	0.0031	0.0082
	10	0.0055	0.0029	0.0013	0.0113	0.0032	0.0011	0.0005	0.0042
	12	0.0051	0.0029	0.0015	0.0114	0.0029	0.0011	0.0009	0.0044
	14	0.0047	0.0029	0.0016	0.0116	0.0076	0.0023	0.0002	0.0076

Sn, Sp, Ac, and MCC denote sensitivity, specificity, accuracy, and Matthews correlation coefficient, respectively

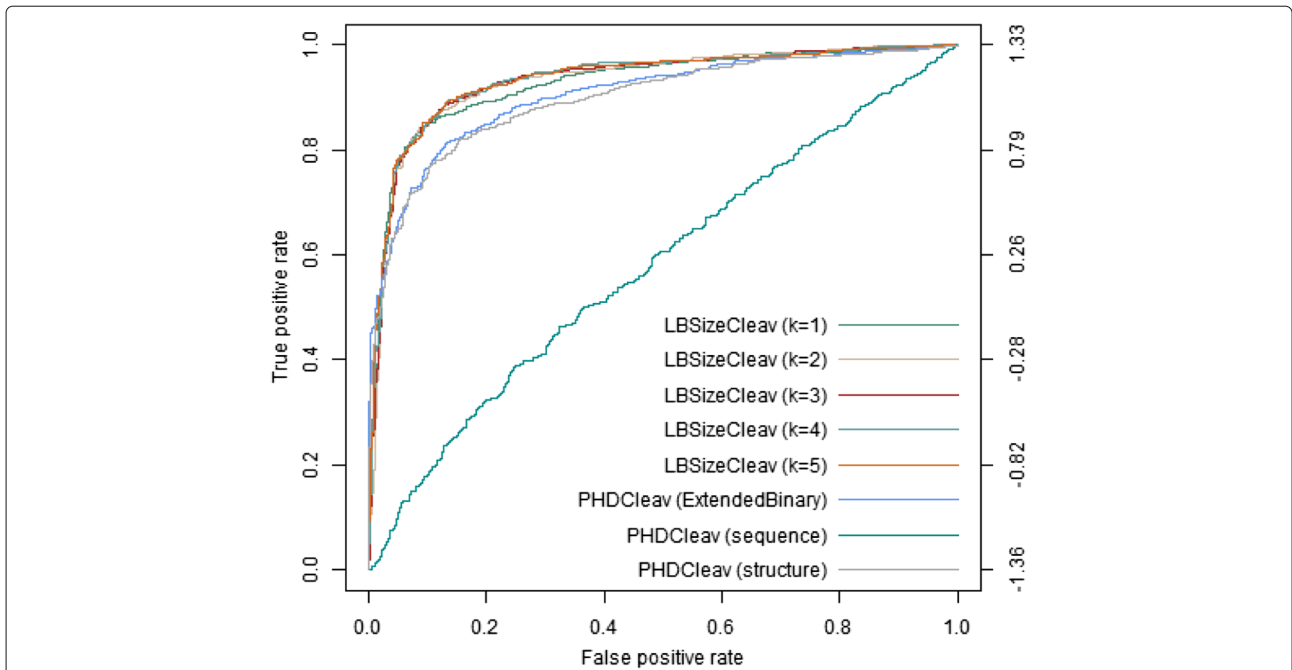


**Fig. 2** Results on ROC curves by LBSizeCleave and PHDCleave with window size  $w = 14$  for 5p arm. From the figure we could see that the ROC curve of LBSizeCleave from  $k = 1$  to  $k = 5$  is significantly better than binary Pattern and extended binary pattern of PHDCleave for both 5p and 3p arms

of prediction accuracy of LBSizeCleave at  $w = 12, 14$  were higher than those of PHDCleave. As for prediction performance in the 3p arm of pre-miRNA, the best result of PHDCleave corresponded to the accuracy of 79.1%, whereas LBSizeCleave achieved the accuracy of 83.0%.

Table 3 shows the results of PHDCleave and LBSizeCleave ( $k = 1, \dots, 5$ ) based on sequences and secondary structures predicted by the RNAFold. In terms of prediction performance in the 5p arm of pre-miRNA, the best result of PHDCleave corresponded to the accuracy of 81.3%,

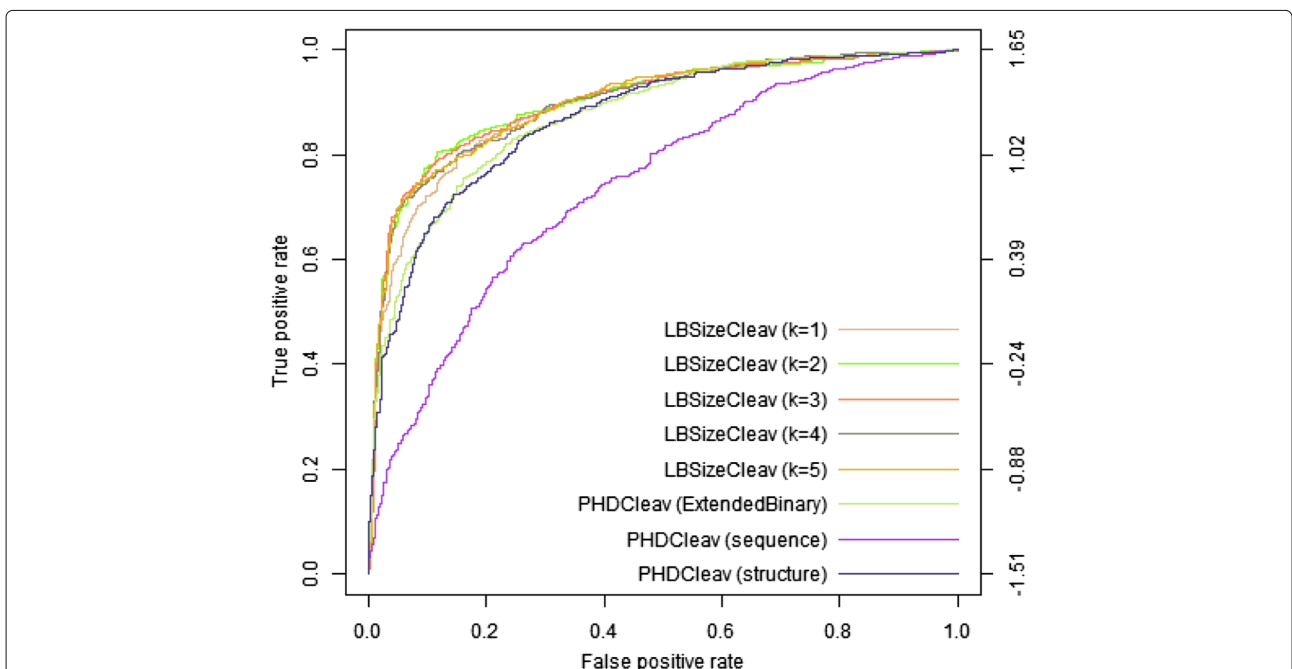


**Fig. 3** Results on ROC curves by LBSizeCleave and PHDCleave with window size  $w = 14$  for 3p arm. From the figure we could see that the ROC curve of LBSizeCleave from  $k = 1$  to  $k = 5$  is significantly better than binary Pattern and extended binary pattern of PHDCleave for both 5p and 3p arms

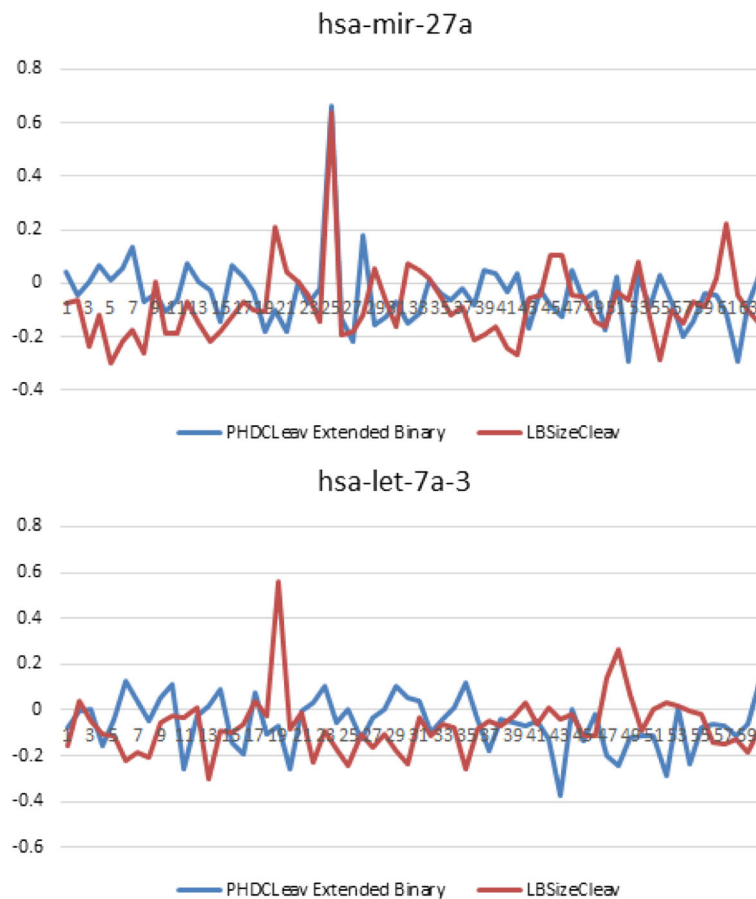


**Fig. 4** Regression analysis examples of LBSIZEcleav( $k = 5$ ) compared with PHDCleav extended binary

whereas LBSIZEcleav at  $k = 1$  achieved the accuracy of 82.2%. As for prediction performance in the 3p arm of pre-miRNA, the best result of PHDCleav corresponded to the accuracy of 82.9%, whereas LBSIZEcleav achieved the accuracy of 85.1%.

To better evaluate the performance we also calculated the variance of each prediction result in Table 4. Figures 2 and 3 show the results of LBSIZEcleav and PHDCleav on receiver-operator characteristic (ROC) curves at window size  $w = 14$  in 5p and 3p arms. Judging by the

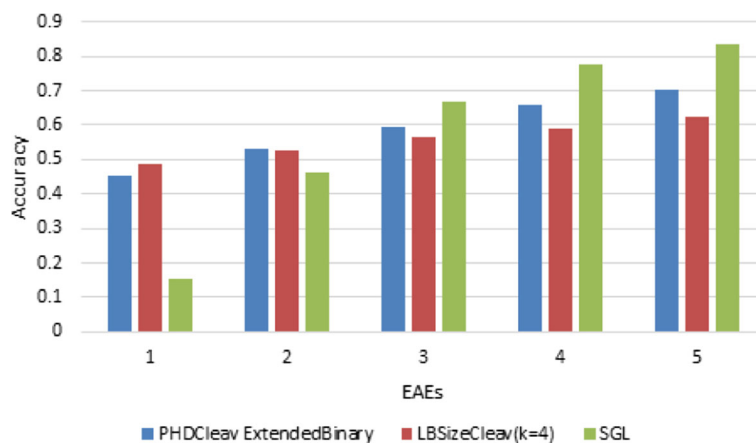


**Fig. 5** Result on accuracy of LBSIZEcleav( $k = 5$ ) compared with PHDCleav extended binary and SGL of prediction in CD-5p



performance evaluation, our newly developed method outperformed the binary patterns of PHDCleav; this finding was suggestive of efficiency of the feature representing the length of loop/bulge structures.

Since in our results, LBSizeCleave with parameters of  $w = 14, k = 5$  outperforms the others, we selected these parameters as our parameters for prediction model. For an input sequence, we created a shift window of size 14 nt shifting from the 5p arm to the 3p arm. For each shift window we performed an SVM regression analysis using our model. Here we randomly selected 2 precursors from

the dataset and showed the score of the extended binary pattern of PHDCleav and LBSizeCleave with  $k = 5$ . From the result we could see that although both tools have predicted the cleavage site correctly, LBSizeCleave predicted more true negatives than extended binary pattern of PHDCleav, which indicates a better performance in identifying negative patterns of LBSizeCleave (see in Fig. 4).

We also compared the performance of our tools with another state-of-art method, a recent published paper introduced an easy way named SGL (Simple Geometric Locator) to calculate the cleavage site of miRNA which

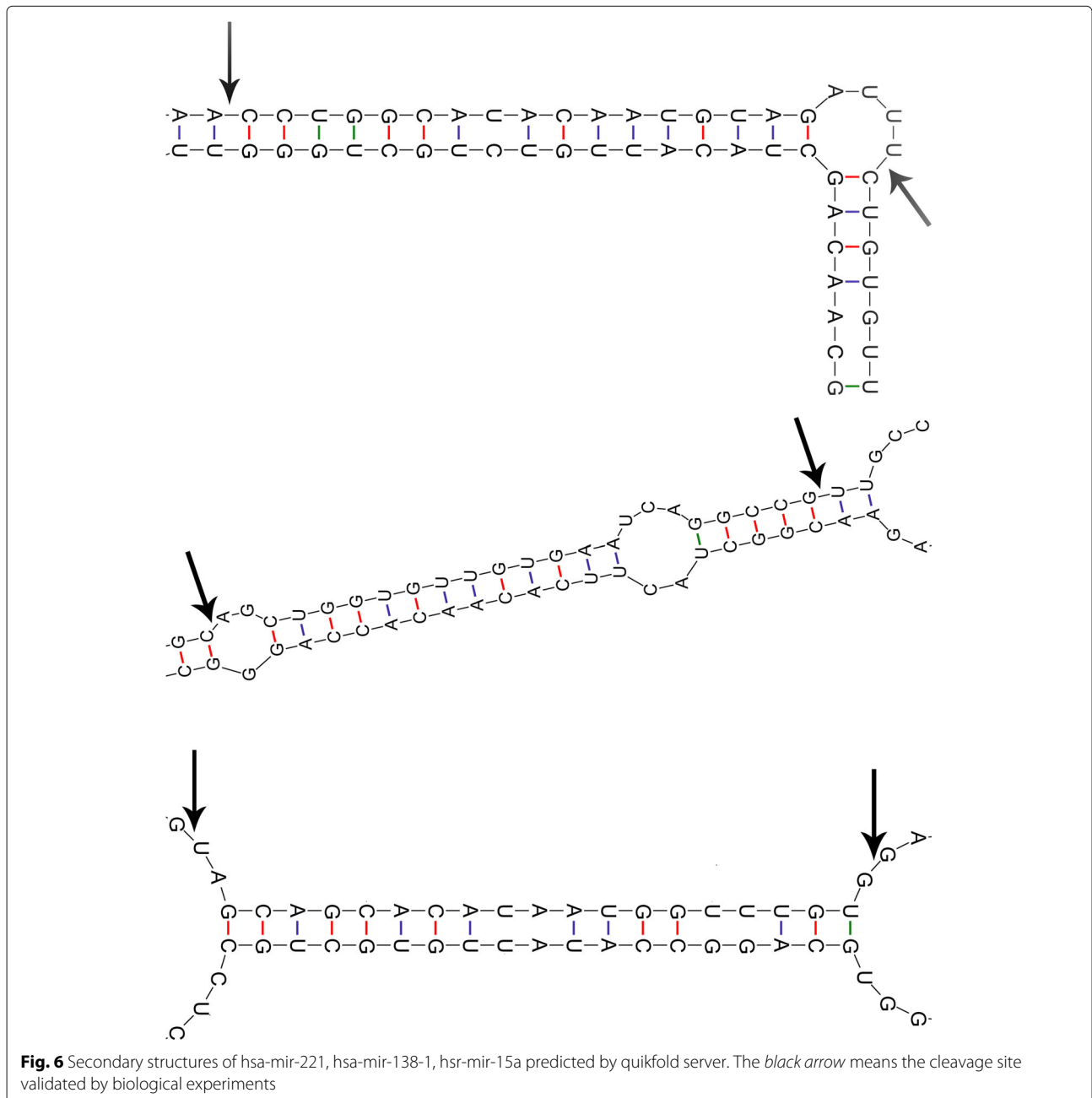


**Table 5** Number of patterns predicted only by LBSizeCleave( $k = 1, 4$ )/PHDCleave(extended binary) using secondary structure predicted by quikfold

		5'-arm	3'-arm
Positive	Only predicted by LBSizeCleave ( $k = 1$ ) compared with PHDCleave (extended binary)	39	39
	Only predicted by PHDCleave (extended binary) compared with LBSizeCleave ( $k = 1$ )	57	38
Negative	Only predicted by LBSizeCleave ( $k = 1$ ) compared with PHDCleave (extended binary)	82	65
	Only predicted by PHDCleave (extended binary) compared with LBSizeCleave ( $k = 1$ )	23	12
Positive	Only predicted by LBSizeCleave ( $k = 4$ ) compared with PHDCleave(extended binary)	39	39
	Only predicted by PHDCleave compared with LBSizeCleave ( $k = 4$ )	57	38
Negative	Only predicted by LBSizeCleave ( $k = 4$ ) compared with PHDCleave(extended binary)	82	65
	Only predicted by PHDCleave (extended binary) compared with LBSizeCleave ( $k = 4$ )	23	12

outperforms other methods. We generated a benchmark to compare our method as well as PHDCleave with SGL of prediction in CD-5p, which result is shown in Fig. 5. In this benchmark we selected the threshold (0.0) of LBSizeCleave as well as PHDCleave and calculated the EAEs(End Absolute Error, the absolute error of the predicted minus the true position for a specific duplex end) from the true cleavage site and compared it with the SGL method. From the result we could see that although at high EAEs PHDCleave outperforms LBSizeCleave, LBSizeCleave outperforms both PHDCleave and SGL at EAE 1, which indicates that LBSizeCleave predicted less false positives than PHDCleave.

**Discussion**

There were several pre-miRNAs, such as pre-mir221, pre-mir138-1, and pre-mir-15a, that were identified by LBSizeCleave but were not identified by PHDCleave in the prediction results from the 5p arm of a pre-miRNA with a shift window of 14 nt (see Fig. 6). By comparing these three pre-miRNAs, we found that all of them contain a part of loop/bulge structures that is more than 1 nt long in their mature parts. This result indicates that the length of a loop/bulge structure is an important determinant of a cleavage site. Careful analysis revealed that pre-mir221 and pre-mir138-1 contain their loop/bulge structures in their bulge parts, whereas pre-mir-15a has its loop/bulge structure in its loop part, proving that both loop and bulge structures can affect the cleavage site selection. To further evaluate the effect of the length of a loop/bulge structure in affecting the cleavage site selection we calculated the number of pre-miRNAs which LBSizeCleave identified successfully while PHDCleave failed to identify and vice versa (see Table 5). From the result we could see that for the positive patterns our method performs almost the same as PHDCleave, but for negative patterns our method shows a significant improvement in accuracy. This result indicates that our method has a better resolution in identifying negative patterns.

**Conclusions**

In this study, we proposed a novel method—LBSizeCleave—for prediction of Dicer cleavage sites. By integrating information on the length of a loop/bulge structure of a pre-miRNA (as predicted by the quikfold server), we developed novel feature space mapping. We performed fivefold cross-validation for validated pre-miRNA sequences from miRBase. In both 5p and 3p arms, the proposed method showed better performance than did the binary patterns of PHDCleave. This study shows a new way of feature evaluation; moreover, the better performance of our method points to the effectiveness of analysis of loop/bulge length at detecting Dicer cleavage sites.

**Abbreviations**

DGCR8: DiGeorge syndrome chromosomal region 8; dsRND: Double-stranded RNA-binding domain; FN: false negative; FP: False positive; miRNA: MicroRNA; PAZ: PIWI, AGO, and Zwillie domain; RISC: RNA-induced silencing complex; SVM: Support Vector Machine; TN: True negative; TP: True positive

**Acknowledgments**

None.

**Funding**

TA was partially supported by Grant-in-Aid # 26240034 from the Japan Society for Promotion of Science (JSPS); MH was in part supported by Grant-in-Aid # 24500361 from JSPS.

**Availability of data and materials**

Related data and source code is available at <http://sunflower.kuicr.kyoto-u.ac.jp/~houu/LBSizeCleave/index.html>.

**Authors' contributions**

YB collected data and implemented the algorithm. MH helped implementation and computational experiment. YB and TA developed the algorithm. TA, MH supervised the whole project. YB carried out data interpretation and finalized the writing. All authors read and approved the final manuscript.

**Competing interests**

The authors declare that they have no competing interests.

**Consent for publication**

Not applicable.

**Ethics approval and consent to participate**

Not applicable.

Received: 11 April 2016 Accepted: 11 November 2016

Published online: 25 November 2016

## References

- Bartel DP. MicroRNAs: genomics, biogenesis, mechanism, and function. *Cell*. 2004;116(2):281–97.
- Bernstein E, Caudy AA, Hammond SM, Hannon GJ. Role for a bidentate ribonuclease in the initiation step of RNA interference. *Nature*. 2001;409(6818):363–6.
- Lee Y, Jeon K, Lee JT, Kim S, Kim VN. MicroRNA maturation: stepwise processing and subcellular localization. *EMBO J*. 2002;21(17):4663–670.
- Zamore PD, Tuschl T, Sharp PA, Bartel DP. RNAi: double-stranded RNA directs the ATP-dependent cleavage of mRNA at 21 to 23 nucleotide intervals. *Cell*. 2000;101(1):25–33.
- Elbashir SM, Harborth J, Lendeckel W, Yalcin A, Weber K, Tuschl T. Duplexes of 21-nucleotide RNAs mediate RNA interference in cultured mammalian cells. *Nature*. 2001;411(6836):494–8.
- Hammond SM, Bernstein E, Beach D, Hannon GJ. An RNA-directed nuclease mediates post-transcriptional gene silencing in *Drosophila* cells. *Nature*. 2000;404(6775):293–6.
- MacRae IJ, Zhou K, Li F, Repic A, Brooks AN, Cande WZ, Adams PD, Doudna JA. Structural basis for double-stranded RNA processing by Dicer. *Science*. 2006;311(5758):195–8.
- Lau PW, Guiley KZ, De N, Potter CS, Carragher B, MacRae IJ. The molecular architecture of human Dicer. *Nat Struct Mol Biol*. 2012;19(4):436–40.
- Park JE, Heo I, Tian Y, Simanshu DK, Chang H, Jee D, Patel DJ, Kim VN. Dicer recognizes the 5 [prime] end of RNA for efficient and accurate processing. *Nature*. 2011;475(7355):201–5.
- Gu S, Jin L, Zhang Y, Huang Y, Zhang F, Valdmann PN, Kay MA. The loop position of shRNAs and pre-miRNAs is critical for the accuracy of dicer processing in vivo. *Cell*. 2012;151(4):900–11.
- Feng Y, Zhang X, Graves P, Zeng Y. A comprehensive analysis of precursor microRNA cleavage by human Dicer. *RNA*. 2012;18(11):2083–092.
- MacRae IJ, Zhou K, Doudna JA. Structural determinants of RNA recognition and cleavage by Dicer. *Nat Struct Mol Biol*. 2007;14(10):934–40.
- Jin Y, Lee CG. Single nucleotide polymorphisms associated with microRNA regulation. *Biomolecules*. 2013;3(2):287–302.
- Ahmed F, Kaundal R, Raghava GP. PHDcleav: a SVM based method for predicting human Dicer cleavage sites using sequence and secondary structure of miRNA precursors. *BMC Bioinforma*. 2013;14(Suppl 14):9.
- Drucker H, Wu D, Vapnik VN. Support vector machines for spam categorization. *IEEE Trans Neural Netw*. 1999;10(5):1048–1054.
- Bhasin M, Raghava G. ESLpred: SVM-based method for subcellular localization of eukaryotic proteins using dipeptide composition and PSI-BLAST. *Nucleic Acids Res*. 2004;32(suppl 2):414–9.
- Cai C, Han L, Ji ZL, Chen X, Chen YZ. SVM-Prot: web-based support vector machine software for functional classification of a protein from its primary sequence. *Nucleic Acids Res*. 2003;31(13):3692–697.
- Zavaljevski N, Stevens FJ, Reifman J. Support vector machines with selective kernel scaling for protein classification and identification of key amino acid positions. *Bioinformatics*. 2002;18(5):689–96.
- Kumar M, Gromiha MM, Raghava G. Prediction of RNA binding sites in a protein using SVM and PSSM profile. *Proteins Struct Funct Bioinforma*. 2008;71(1):189–94.
- Ng KLS, Mishra SK. De novo SVM classification of precursor microRNAs from genomic pseudo hairpins using global and intrinsic folding measures. *Bioinformatics*. 2007;23(11):1321–1330.
- Burbidge R, Trotter M, Buxton B, Holden S. Drug design by machine learning: support vector machines for pharmaceutical data analysis. *Comput Chem*. 2001;26(1):5–14.
- Byvatov E, Fechner U, Sadowski J, Schneider G. Comparison of support vector machine and artificial neural network systems for drug/nondrug classification. *J Chem Inf Comput Sci*. 2003;43(6):1882–1889.
- Lyngsø RB, Zuker M, Pedersen CN. Internal loops in RNA secondary structure prediction. In: *Proceedings of the Third Annual International Conference on Computational Molecular Biology*. New York: ACM; 1999. p. 260–7.
- Griffiths-Jones S, Grocock RJ, Van Dongen S, Bateman A, Enright AJ. miRBase: microRNA sequences, targets and gene nomenclature. *Nucleic Acids Res*. 2006;34(suppl 1):140–4.
- Markham NR, Zuker M. UNAFold. In: *Bioinformatics*. Springer; 2008. [http://link.springer.com/protocol/10.1007/978-1-60327-429-6\\_1](http://link.springer.com/protocol/10.1007/978-1-60327-429-6_1).
- Hofacker IL. Vienna RNA secondary structure server. *Nucleic Acids Res*. 2003;31(13):3429–431.
- Chang CC, Lin CJ. LIBSVM: A library for support vector machines. *ACM Trans Intell Syst Technol (TIST)*. 2011;2(3):27.

Submit your next manuscript to BioMed Central and we will help you at every step:

- We accept pre-submission inquiries
- Our selector tool helps you to find the most relevant journal
- We provide round the clock customer support
- Convenient online submission
- Thorough peer review
- Inclusion in PubMed and all major indexing services
- Maximum visibility for your research

Submit your manuscript at  
[www.biomedcentral.com/submit](http://www.biomedcentral.com/submit)

